Advance Publication Cover Page

Packing Structure Effects on the Slow Magnetic Relaxation Pathways of Dysprosium (III) Complexes

Mritunjoy Kamila, Goulven Cosquer,* Brian K. Breedlove, and Masahiro Yamashita*

Advance Publication on the web February 24, 2017
doi:10.1246/bcsj.20160408

Packing Structure Effects on the Slow Magnetic Relaxation Pathways of Dysprosium (III) Complexes

Mritunjoy Kamila,[1] Goulven Cosquer,* [1,2] Brian K. Breedlove,[1,2] Masahiro Yamashita* [1,2,3]

[1] Department of Chemistry, Graduate School of Science, Tohoku University, 6-3 Aramaki-Aza-Aoba, Aoba-ku, Sendai 980-8578, Japan

[2] Core Research for Evolutional Science and Technology (CREST), Japan Science and Technology (JST), 4-1-8 Kawaguchi, Saitama 332-0012, Japan

[3] WPI Research Center, Advanced Institute for Materials Research, Tohoku University, 2-1-1 Katahira, Aoba-ku, Sendai 980-8577, Japan

E-mail: <cosquer.g@m.tohoku.ac.jp> <yamasita.m@gmail.com>

Abstract

Three complexes, [Dy{5-(5-methylthiophen-2-yl)-2,2'-bipyridine}(hfac)$_3$] (**6**), [Dy{5-(4-bromo-5-methylthiophen-2-yl)-2,2'-bipyridine}(hfac)$_3$] (**7**) and [Dy{5-(4-ethynyl-5-methylthiophen-2-yl)-2,2'-bipyridine}(hfac)$_3$] (**8**) (hfac = hexafluoroacetylacetate), were synthesized to investigate the effects of substituents on the ligand far from the metal ion on the magnetic properties of the dysprosium ion. **7** crystallized in two polymorphs ($P2_1/n$ for **7a** and $P2_1/a$ for **7b**), whereas **6** and **8** crystallized in one polymorph ($P2_1/n$ and $P2_1/a$, respectively). All of the complexes have columnar structures, and in **6** and **7a**, there are π–π stacking interactions between neighboring aromatic rings in contrast to compounds **7b** and **8**, which do not show such interactions. Every complex underwent slow magnetic relaxation with a single relaxation time, except for complex **7a**, for which there were two relaxation times. In order to clarify the role of distal substitution and crystal packing, the magnetic properties were studied in solution, where all of the complexes show single relaxation times.

1. Introduction

In the early 1990s, the first single-molecule magnet (SMM), $Mn_{12}Ac$, was discovered.[1] This molecule behaves as a tiny molecular magnet, retaining its magnetization for a long time at liquid helium temperatures. This complex shows hysteresis due to bistability of the magnetic unit, which can be used in data storage devices.[2] Since then, many polynuclear transition metal complexes showing SMM behavior were reported. In contrast to SMMs of transition metal ions, where the presence of hysteresis is mainly due to the superexchange interactions between the ions, lanthanide ions have intrinsic anisotropy, allowing them to retain their magnetization without interactions. In 2003, a single ion lanthanide double-decker complex was reported to exhibit SMM behavior.[3]

The magnetic properties of lanthanide ions, which are attributed to the 4*f* orbital and the splitting of the ground state to m_J levels by the crystal field, are easily tuned by slightly modifying the coordination polyhedron. Modification can be done by directly changing the first coordination sphere, by adjusting the size of counter ions,[4] or by incorporating hydrogen bonds with the atoms in the first coordination sphere. In the case of hydrogen bonding, a slight modification of the coordination sphere induce a total on/off switching of the slow magnetic relaxation, and SMM behavior only occurs in absence of hydrogen bond.[5] Another way to tune the magnetic properties of lanthanide ions has been investigated using a series of Fe_2Dy_2 coordination clusters.[6] By changing the interactions among the Fe and Dy ions and by modifying the ligand coordinated to the Fe ion, the direction of the easy magnetization axis of the Dy ion can be changed.

Since the crystal field decreases proportionally with the square of the distance between the ions, previous work has focused on changing the first or second coordination sphere to tune the magnetic properties. Instead of investigating the substitution or the modification of the coordination atoms, we studied the effects of distal substituents on the ligand regardless of the coordination site. The substituents will induce a change in the crystal packing which will affect the coordination sphere in the crystals.

A family of ligands in which 2,2'-bipyridine and methylthiophene with proton (**1**), bromine (**3**) or acetylene (**5**) group on the 4-position of the thiophene ring was prepared. The bipyridyl group can coordinate to Dy(hfac)$_3$(H_2O)$_2$ (hfac = hexafluoroacetylacetonate ion) to form a mononuclear complex (**6**, **7** and **8**, respectively). At the same time, the thiophene ring acts as an antenna to enhance the luminescence of the Dy ion. Luminescence spectra of lanthanide ion combined with static magnetic measurements provide an excellent way to determine and precisely analyze the energy splitting of the ground state.[7] Crystal structures and optical and magnetic properties of the four complexes were investigated.

Complex **7** crystallized in two different space groups (**7a** and **7b**), and one of them (**7b**) was isostructural with **8**. The differences in the structures help us to determine more accurately the role of the crystal structure in the slow relaxation of the magnetization of the Dy ion. The magnetic susceptibilities of the four crystalline compounds were frequency dependent with and without an external magnetic field. To understand the effects of substitutents and/or crystal packing on the magnetic properties of the Dy ion, the magnetic properties of the complexes were measured in solution to remove the effects of the crystal field on the magnetism.

2. Experimental

General considerations. All of the chemicals and solvents

used in this study were obtained from Sigma Aldrich, Tokyo Chemical Industry, Strem or Wako Chemicals GmbH. $Dy(hfac)_3{\cdot}2H_2O$ was prepared according to the literature.[8] Elemental analyses for C, N, and H were performed on a Perkin-Elmer 240C elemental analyzer (PerkinElmer, Waltham, MA, USA) at the Research and Analytical Centre for Giant Molecules, Tohoku University.

*Synthesis of 5-(5-methylthiophen-2-yl)-2,2'-bipyridine (**1**).*
5-bromo-2,2'-bipyridine (0.480 g, 2 mmol), 2-methylthiophene (0.401 g, 4 mmol) and KOAc (0.401 g, 4 mmol) in dry DMA (5 ml) were stirred under N_2 at 150 °C during 20 h in presence of $Pd(OAc)_2$ (0.009 g, 2 mol%). After cooling the solution to room temperature, CH_2Cl_2 (15 ml) and an aqueous saturated NH_4Cl solution (10 ml) were added. The reaction solution was extracted three times with 15 ml of CH_2Cl_2, and the combined organic layers were washed three times with 10 ml of water. The solvent was evaporated under reduced pressure, and the crude product was purified by using column chromatography (silica; 5:1 v/v hexane:EtOAc) to afford compound 1 in 22% yield (111 mg). ^{1}H NMR ($CDCl_3$, 500 MHz): δ 8.89 (dd, 1H, *J* = 2.3 and 0.6 Hz, ArH), 8.68 (ddd, 1H, *J* = 4.7, 1.7 and 0.8 Hz, ArH), 8.44–8.36 (m, 2H, ArH), 7.93 (dd, 1H, *J* = 8.3 and 2.4 Hz, ArH), 7.82 (td, 1H, *J* = 7.8 and 1.8 Hz, ArH), 7.30 (ddd, 1H, *J* = 7.4, 4.8 and 1.1 Hz, ArH), 7.24 (d, 1H, *J* = 3.5 Hz, ArH), 6.82–6.77 (m, 1H, ArH), 2.54 (s, 3H, $ArCH_3$) ppm. HR-MS (ESI+) m/z $[M + H]^+$ calcd. for $[C_{15}H_{13}N_2S]^+$ 253.0799; found: 253.0803.

*Synthesis of (4-bromo-5-methylthiophen-2-yl)boronic acid (**2**).*
3,5-dibromo-2-methylthiophene (2.56 g, 10 mmol) was dissolved in anhydrous diethyl ether (80 ml) in a two neck round bottom flask under a N_2 atmosphere at −78 °C, and then an n-butyllithium solution (2.5 M) in hexane (6.6 ml, 10.5 mmol) was added dropwise while stirring. After 30 min, triisopropyl borate (2.35 g, 25 mmol) was added dropwise, and the solution was stirred at −78 °C for 4 h before being allowed to warm to ambient temperature overnight. After 15 h, the reaction mixture was shaken with hydrochloric acid (1.2 N, 50 ml), and the ether phase separated and extracted with aqueous sodium hydroxide (1 N, 4 × 50 ml). The combined aqueous phase was then filtered to remove traces of solid and then acidified to pH = 1 at 0 °C with hydrochloric acid (10^{-2} M). The product was dried in vacuo to yield boronic acid 4 as a white powder (1.81 g, 82%). ^{1}H NMR (CD_3OD, 500 MHz): δ 8.30 (s, 2H, BOH), 7.50 (s, 1H, ArH), 2.37 (s, 3H, $ArCH_3$) ppm. HR-MS (ESI+) m/z $[M - H]^-$ calcd. for $[C_5H_5BBrO_2S]^-$ 218.9288 and 220.9263; found: 218.9252 and 220.9153.

*Synthesis of 5-(4-bromo-5-methylthiophen-2-yl)-2,2'-bipyridine (**3**).*
Compound 2 (2.319 g, 10.5 mmol), 5-bromo-2,2'-bipyridine (2.351 g, 10 mmol), Na_2CO_3 (2.12 g, 10 mmol) and $Pd(PPh3)_4$ (0.346 g, 0.3 mmol) were refluxed under N_2 at 100 °C for 20 h in a degassed mixture of toluene (100 ml), ethanol (100 ml) and water (50 ml). After the solution was cooled to room temperature, 50 ml of an aqueous saturated NH_4Cl solution was added, and the solution was extracted three times with 100 ml of CH_2Cl_2. The organic layer were combined, and the solution was washed with brine solution. The solvent was evaporated under reduced pressure. The crude product was purified by using column chromatography over silica (4:1 v/v hexane:EtOAc), affording 3 in 83% yield (2.749 g). ^{1}H NMR ($CDCl_3$, 500 MHz): δ 8.86–8.83 (m, 1H, ArH), 8.69 (ddd, 1H, *J* = 4.8, 1.7 and 0.9 Hz, ArH), 8.44–8.38 (m, 2H, ArH), 7.90 (dd, 1H, *J* = 8.3 and 2.4 Hz, ArH), 7.82 (td, 1H, *J* = 7.7 and 1.8 Hz, ArH), 7.31 (ddd, 1H, *J* = 7.5, 4.8 and 1.2 Hz, ArH), 7.23 (s, 1H, ArH), 2.46 (s, 3H, $ArCH_3$) ppm. HR-MS (ESI+) m/z $[M + H]^+$ for $[C_{15}H_{12}BrN_2S]^+$ 330.9904 and 332.9884; found: 330.9915 and 332.9902.

*Synthesis of 5-(4-((trimethylsilyl)ethynyl)-5-methylthiophen-2-yl)-2,2'-bipyridine (**4**).*
Compound 3 (0.298 g, 0.9 mmol), ethynyltrimethylsilane (0.098 g, 1 mmol), $PdCl_2$ (0.008 g, 0.05 mmol), PPh_3 (0.073 g, 0.28 mmol), CuI (0.0095 g, 0.05 mmol), diethylamine (1.5 ml, 13.6 mmol) and dry DMF (0.5 ml) were stirred under N_2 in a heavy-walled Smith process vial at 120 °C for 30 min in a microwave reactor. The mixture was treated with diethyl ether, filtered, and poured into 0.1 M aqueous HCl (10 ml). The resulting solution was extracted three times with diethyl ether (10 ml). The combined organic layers were washed with water and then concentrated under reduced pressure. The residue was treated with hexane and filtered through Celite. The solvent was evaporated, affording 4 in 89% yield (0.279 g). ^{1}H NMR ($CDCl_3$, 500 MHz): δ 8.85 (s, 1H, ArH), 8.6 (d, 1H, *J* = 4.1 Hz, ArH), 8.40 (d, 2H, *J* = 8.2 Hz, ArH), 7.90 (dd, 1H, *J* = 8.3 and 2.4 Hz, ArH), 7.81 (td, 1H, *J* = 7.8 and 1.8 Hz, ArH), 7.32–7.29 (m, 2H, ArH), 2.56 (s, 3H, $ArCH_3$) 0.26 (s, 9H, $SiCH_3$) ppm. HR-MS (ESI+) m/z $[M + H]^+$ calcd. for $[C_{20}H_{21}N_2SSi]^+$ 349.1195; found 349.1201.

*Synthesis of 5-(4-ethynyl-5-methylthiophen-2-yl)-2,2'-bipyridine (**5**).*
Compound 4 (0.279 g, 0.8 mmol) and K_2CO_3 (0.221 g, 1.6 mmol) in methanol (30 ml) were stirred overnight at room temperature. The product was separated by using column chromatography on silica with CH_2Cl_2 as eluent to afford 5 in 98% yield (0.217 g). ^{1}H NMR ($CDCl_3$, 500 MHz): δ 8.86 (dd, 1H, *J* = 2.3 and 0.7 Hz, ArH), 8.68 (ddd, 1H, *J* = 4.8, 1.7 and 0.9 Hz, ArH), 8.44–8.38 (m, 2H, ArH), 7.91 (dd, 1H, *J* = 8.3 and 2.4 Hz, ArH), 7.82 (td, 1H, *J* = 7.7 and 1.8 Hz, ArH), 7.34–7.29 (m, 2H, ArH), 3.23 (s, 1H, CCH), 2.59 (s, 3H, $ArCH_3$) ppm. HR-MS (ESI+) m/z $[M-H]^-$ calcd. for $[C_{17}H_{11}N_2S]^-$ 275.0643; found 275.0619.

*Synthesis of complex **6**.*
$Dy(hfac)_3{\cdot}2H_2O$ (24 mg, 0.03 mmol) was dissolved in boiling heptane (10 ml). After the solution was allowed to cool to 60 °C, a dichloromethane solution (5 ml) of ligand 1 (7.57 mg, 0.03 mmol) was added, and the solution was stirred at room temperature for 10 min. Slow evaporation of the solvent at room temperature over a few days gave a pale yellow needle shaped crystals of **6** suitable for single crystal x-ray diffraction. Yield: 75% (23.3 mg). Anal. Calcd for $C_{30}H_{15}DyF_{18}N_2O_6S$: C, 34.78; H, 1.46; N, 2.70. Found: C, 34.97; H, 1.62; N, 2.90.

*Synthesis of complex **7**.*
$Dy(hfac)_3{\cdot}2H_2O$ (24 mg, 0.03 mmol) was dissolved in boiling heptane (10 ml). After the solution was allowed to cool to 60 °C, a dichloromethane solution (5 ml) of ligand 3 (9.94 mg, 0.03 mmol) was added, and the solution was stirred at room temperature for 10 min, giving complex 7. Slow evaporation of the solvent at room temperature over a few days gave a pale yellow needle crystal of **7a**. Hexagonal block shaped crystal of **7b** was obtained by slow evaporation of the mother liquor at 30 °C for 1 week. Yields: 75% (25.1 mg) for 7a and 72% (24.1 mg). Anal. Calcd for $C_{30}H_{14}BrDyF_{18}N_2O_6S$: C, 32.32; H, 1.27; N, 2.51. Found: C, 32.29; H, 1.36; N, 2.50.

*Synthesis of complex **8**.*
$Dy(hfac)_3{\cdot}2H_2O$ (24 mg, 0.03 mmol) was dissolved in boiling heptane (10 ml). After the solution was allowed to cool to 60 °C, a dichloromethane solution (5 ml) of ligand 5 (8.29 mg, 0.03 mmol) was added, and the solution was stirred at room temperature for 10 min. Slow evaporation of the solvent at room temperature over a few days gave a pale yellow needle crystal of **8** suitable for single crystal x-ray diffraction. Yields: 70% (22.3 mg). Anal. Calcd for $C_{32}H_{15}DyF_{18}N_2O_6S$: C, 36.26; H, 1.43; N, 2.64. Found: C, 36.31; H, 1.42; N, 2.74

.

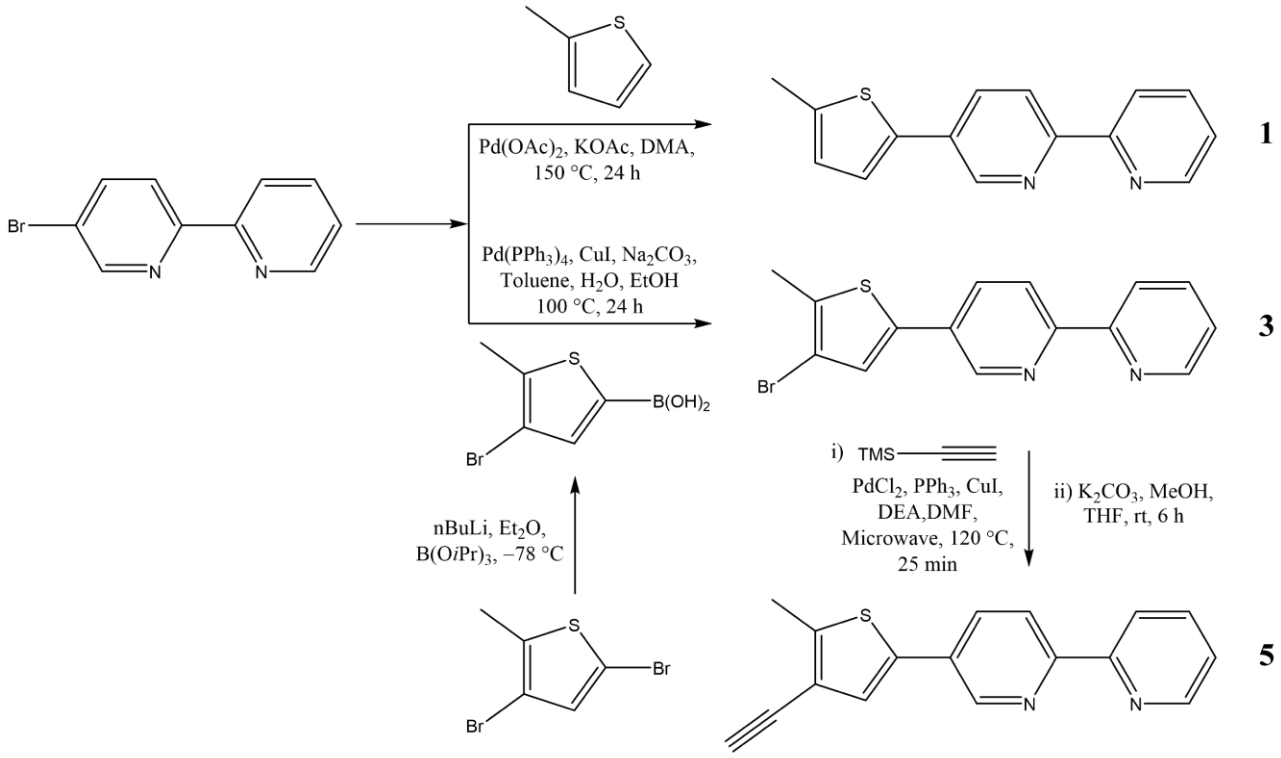

Figure 1. Synthesis of ligands **1**, **3** and **5**.

Single-Crystal X-ray diffraction.

All single-crystal crystallographic data were collected on a Rigaku Saturn70 CCD diffractometer with graphite-monochromated Mo Kα radiation (λ = 0.71075 Å) produced by a VariMax micro-focus X-Ray rotating anode source at 90 K. Data processing was performed using the CrystalClear crystallographic software package.[9] The structures were solved by using direct methods via SIR-92 or SIR-2011.[10] Refinement and further calculations were carried out using WinGX 2013.3 package[11] and SHELXL-2013.[12] The non-H atoms were refined anisotropically using weighted full-matrix least-squares on F^2. H atoms attached to the C atoms were positioned using idealized geometries and refined using a riding model.

Physical Measurements.

Magnetic susceptibility measurements were performed on solid polycrystalline samples on a Quantum Design MPMS-XL SQUID magnetometer. The experimental data were corrected for the diamagnetism of the sample holder, and the intrinsic diamagnetism of the materials was evaluated using Pascal's tables.[13] Ac measurements were performed in a 3 Oe oscillating magnetic field with and without a static dc field. For the solution state magnetic measurements, around 1 cm (0.2 ml) of solution was added to a NMR tube. The masses of the sample and the solvent were measured after the measurement and confirmed with the values from the MH curve in solid and solution states: 4.5 mg for **6**, 5 mg for **7** and 2.8 mg for **8**.

3. Results and Discussion

A series of methylthiophen-bipyridine ligands with a proton, bromine or acetylene substitutent at the 4th position of the thiophene ring were synthesized (Figure 1), and four complexes with Dy(hfac)$_3$ (hfac = hexafluoroacetylacetonato) were prepared and characterized. Complex **7a** was crystallized in the same $P2_1/n$ space group as that of **6** but with two molecules per asymmetric unit instead of one. In contrast, complexes **7b** and **8** are isostructural and crystallized in the $P2_1/a$ space group. Therefore, we will only discuss complex **8**.

Crystal Structure Analysis.

Complex **6** crystallized in the monoclinic space group $P2_1/n$ (Table 2). The asymmetric unit of the complex is composed of one Dy(III) ion, one ligand **1** and three hfac (Figure 2). The Dy ion is coordinated by two nitrogen atoms of ligand **1** and six oxygen atoms from the three hfac with a distorted D_{4d} square anti-prism coordination geometry (Figure 3 and Table 1). Ligand **1** is almost planar with an angle of 2.87° between the two pyridine rings and 2.89° between the thiophene and central pyridine ring. The sulfur atom of the thiophene ring is in a trans configuration with the nitrogen atoms of the pyridine rings.

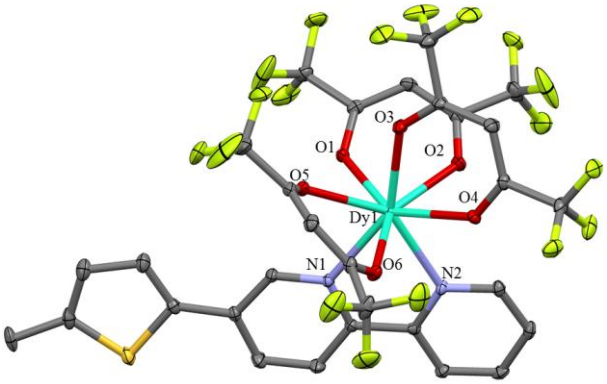

Figure 2. ORTEP drawing of the asymmetric unit of **6**. Thermal ellipsoids are drawn at 30% probability. H atoms are omitted for clarity.

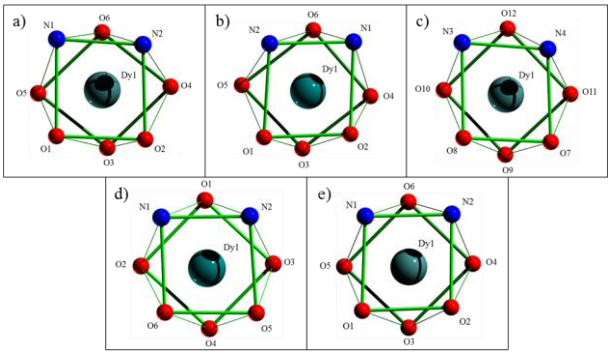

Figure 3. Representation of the coordination polyhedra of the Dy ion in (a) **6**, (b and c) **7a**, (d) **7b** and (e) **8**.

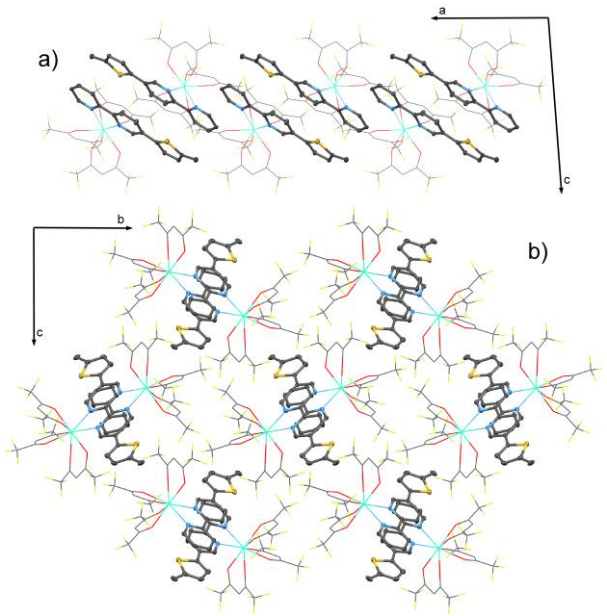

Figure 4. Crystal packing of **6** in (a) the *ac* and (b) *bc* planes. Dysprosium and hfac ligands are displayed as wireframes and ligand **1** as balls and sticks.

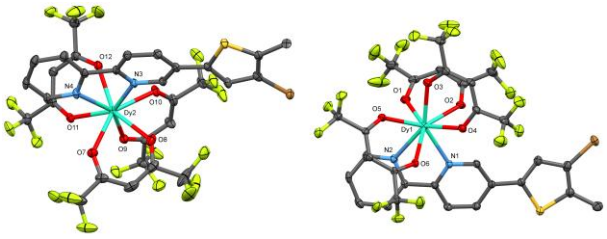

Figure 5. ORTEP drawing of the asymmetric unit of **7a**. Thermal ellipsoids are drawn at 30% probability. H atoms and the disorder of the atoms are omitted for clarity.

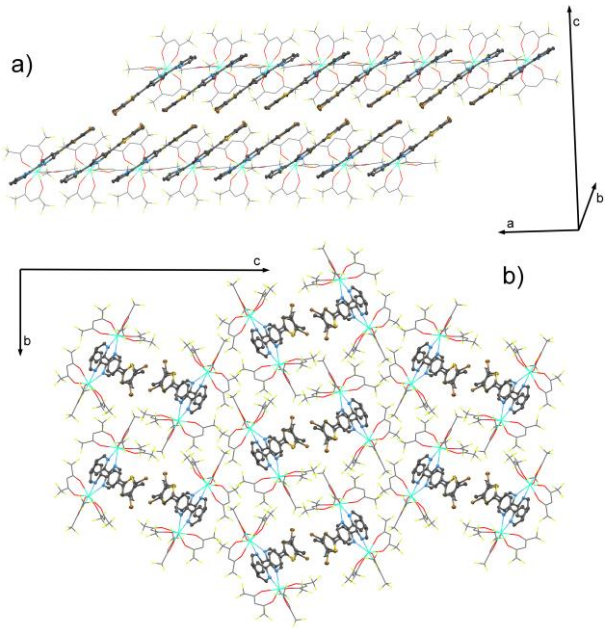

Figure 6. Crystal packing of **7a** in (a) the *ab* and (b) *bc* planes.

An inversion center generates a head-to-tail dimer with π-π interactions between neighboring ligands of the dimer. The average distance between ligands in the dimer was determined to be 3.522 Å (Figure 4). The dimer forms one dimensional columns along the *a* axis through π-π interactions with a mean distance between the pyridine ring of neighboring dimers of 3.316 Å. The columns are isolated from each other by alternating Dy(hfac)$_3$ units. The minimum distance between two Dy ions was determined to be 8.997 Å. Complex **7a** crystallized in the monoclinic space group $P2_1/n$ (Table 2). The asymmetric unit of the complex is composed of two independent molecules. Each of them has a Dy ion coordinated to one ligand **3** through the nitrogen atoms and three hfac through the oxygen atoms (Figure 5). In both molecules, the Dy ion have a distorted D_{4d} square antiprism coordination geometry (Figure 3 and Table 1). The thiophene moieties of the molecules are disordered at two positions due to *cis* and *trans* configurations, unlike the bipyridine rings. **3** is more distorted than **1** is in complex **6**. For **1** and **3**, the angles between the two pyridine rings were 15.57° and 18.15° and between the thiophene and pyridine rings were 3.77° and 9.42°, respectively. **7a** did not dimerize. However, it formed a tail-to-tail double column (Figure 6) with π-π interactions in the column with distances of 3.474 Å and 3.485 Å between the ligands. The distance between two nearest Dy ions was determined to be 9.366 Å. The columns are isolated from each other

by alternating Dy(hfac)$_3$ units.

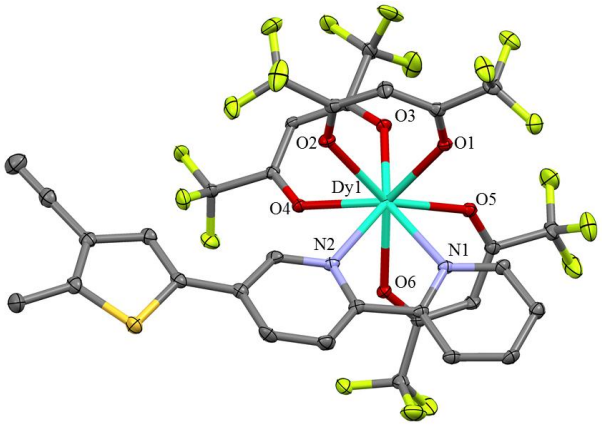

Figure 7. ORTEP drawing of the asymmetric unit of **8**. Thermal ellipsoids are drawn at 30% probability. H atoms are omitted for clarity

Complex **8** crystallized in the monoclinic space group $P2_1/a$ (Table 2). The asymmetric unit of the complex is composed of one Dy ion, one ligand **5** and three hfac ligands (Figure 7). The Dy ion has nearly a D_{4d} square antiprism coordination geometry with six oxygen atoms from the three hfac and two nitrogen atoms of ligand **5** (Figure 3 and Table 1). **5** is distorted with an angle of 12.35° between the two pyridine rings and 5.34° between the thiophene and pyridine rings. This complex forms a regular column with π-π interactions (3.640 Å) between neighboring ligands. The distance between two nearest Dy ions was determined to be 8.688 Å. Like in **6** and **7a**, the columns are isolated from each other by alternating Dy(hfac)$_3$ units.

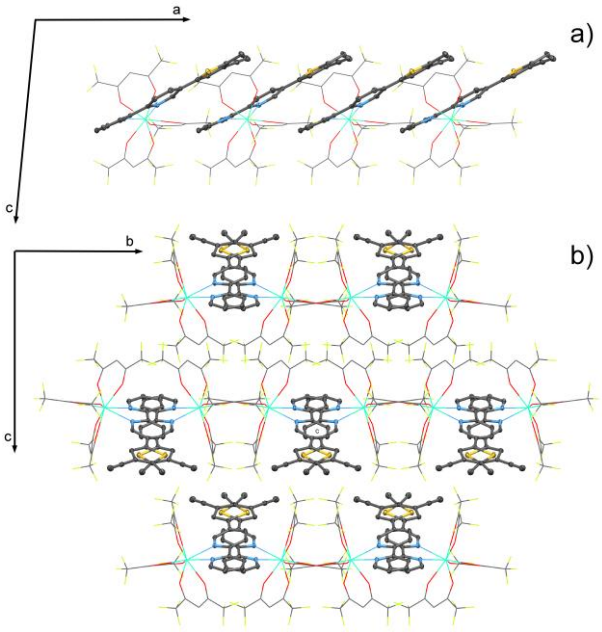

Figure 8. Crystal packing of **8** in (a) the *ac* and (b) *bc* planes.

Table 1. Possible geometries obtained using SHAPE 2.1.[14] Lower values indicate a better agreement between real and ideal geometry.

		6	**7a**		**7b**	**8**
		Dy1	Dy1	Dy2	Dy1	Dy1
SAPR-8	D_{4d}	1.181	0.965	0.521	0.498	0.478
BTPR-8	C_{2v}	1.551	1.967	1.801	2.176	2.145
JBTPR-8	C_{2v}	2.353	2.719	2.240	2.639	2.611
TDD-8	D_{2d}	1.242	1.104	2.112	2.117	2.156

Table 2. X-ray data for the complexes

	6	7a	7b	8
Formula	$C_{30}H_{15}N_2O_6F_{18}SDy$	$C_{30}H_{14}N_2O_6F_{18}SBrDy$	$C_{30}H_{14}N_2O_6F_{18}SBrDy$	$C_{32}H_{15}N_2O_6F_{18}SDy$
M_r (g mol^{-1})	1036.0	1114.9	1114.9	1060.0
Crystal system	Monoclinic	Monoclinic	Monoclinic	Monoclinic
Space group	$P2_1/n$	$P2_1/n$	$P2_1/a$	$P2_1/a$
a (Å)	12.299 (3)	12.621 (3)	15.287 (2)	15.210(3)
b (Å)	15.615 (4)	41.498 (9)	12.307 (2)	12.359(2)
c (Å)	18.656 (5)	14.657 (3)	19.974 (3)	19.882(3)
β (°)	94.454 (4)	99.549 (2)	94.407 (2)	95.275(2)
V (Å^3)	3572 (2)	7570 (3)	3746 (1)	3721 (1)
Z	4	8	4	4
Z'	4	4	4	4
T (K)	93	93	93	93
Diffraction reflection	$4.01 \leq 2\theta \leq 27.54$	$3.05 \leq 2\theta \leq 27.55$	$4.17 \leq 2\theta \leq 27.48$	$3.05 \leq 2\theta \leq 27.49$
Number of reflections	13723	17503	19159	18625
Independent reflections	8033	17228	8593	8442
Number of variables	583	1169	532	541
R_{int}, $R1$, w$R2$ (%)	2.88, 3.03, 7.38	5.82, 6.14, 12.87	4.68, 3.40, 7.76	3.80, 3.93, 8.50

Optical Properties.

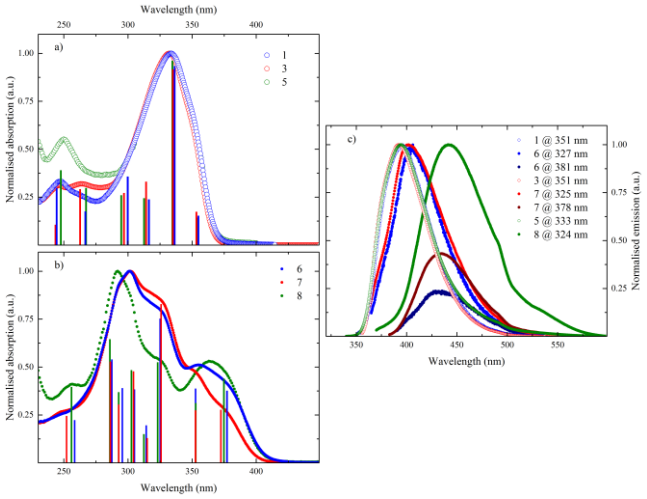

Figure 9. Comparison of the UV-Vis spectra of (a) **1**, **3** and **5** and (b) **6**, **7** and **8**. Bars represent the position and intensity of peaks obtained by Gaussian deconvolution. c) Comparison of the luminescence of **1**, **3**, **5**–**8**.

Optical properties were measured in dichloromethane solution (Figure 9 and S2). Experimental data were fit by using a sum of Gaussian functions. The three ligands have similar absorption spectra with the main absorption centered around 335 nm and five additional absorption around 354, 314, 297, 265 and 245 nm (Table S2). After complexation of the $Dy(hfac)_3$ unit, two additional bands appeared. The band centered around 304 nm was attributed to an intra hfac transition.[15] The second additional peak was centered at 374 nm. In addition, the main transition at 335 was blue-shifted by 10 nm, and the two transitions at 265 and 245 nm were red-shifted by 20 and 10 nm, respectively.

When the ligands were irradiated in the main absorption band, luminescence centered at 396, 391 and 394 nm for ligands **1**, **2** and **5**, respectively, was observed. On the basis of the ligand luminescence, the emissions of complexes **6** and **7** are red-shifted by about 10 nm at 405 and 402 nm, respectively. Irradiation at the wavelength of the lowest energy band of complexes **6** and **7** induced an additional weaker emission centred at 432 and 434 nm, respectively. For **8**, a single emission, red-shifted by about 10 nm in comparison to the two other complexes, was observed at 442 nm. No emission was observed around 400 nm for complex **8**, and computational investigations are in progress to determine the reason.

All three complexes did not show luminescence from the Dy ion at room temperature nor liquid nitrogen temperature (77 K). Several reasons can explain the absence of luminescence from the dysprosium ion:[16] (i) the energy level of the triplet state of the ligand is too low to sensitize the emission level of the ion; (ii) the energy gap between the triplet state of ligand and the emission level of the ion is too small to avoid a feedback of the energy from the ion to the ligand; (iii) the lifetime of the triplet state is shorter than the time needed to excite the ion.

Magnetic properties.

The T dependence of the magnetic susceptibilities (χT) of the complexes are shown in Figure 10. The complexes exhibited similar behavior. For complexes **6**, **7a**, **7b** and **8**, the χT values at 300 K were 14.18, 14.19, 14.17 and 14.18 $cm^3\,K\,mol^{-1}$, respectively, which agree with the expected value for one free Dy ion (14.17 $cm^3\,K\,mol^{-1}$).[17] With a decrease in T, χT decreased to 10.38, 11.20, 10.51 and 10.81 $cm^3\,K\,mol^{-1}$, respectively, at 2 K. The decrease in χT was attributed to the depopulation of the m_J levels of the $^6H_{15/2}$ ground-state multiplet of the Dy^{III} ions. In the four complexes, the coordination spheres of the Dy ion are almost identical (Figure S1), which explains the similarities in the χT curves. The slight differences were attributed to the differences in the energy splitting of the m_J sub-levels of the ground state, which is due to the slight differences in the crystal field around the metal ions.

Magnetization curves at 2 K for the four complexes are also similar to each other with pseudo-saturation from 1 T. The magnetization values for **6**, **7a**, **7b** and **8** at 5 T were determined to be 4.97, 5.13, 5.17 and 5.20 Nβ, respectively. No hysteresis was observed for any of the complexes.

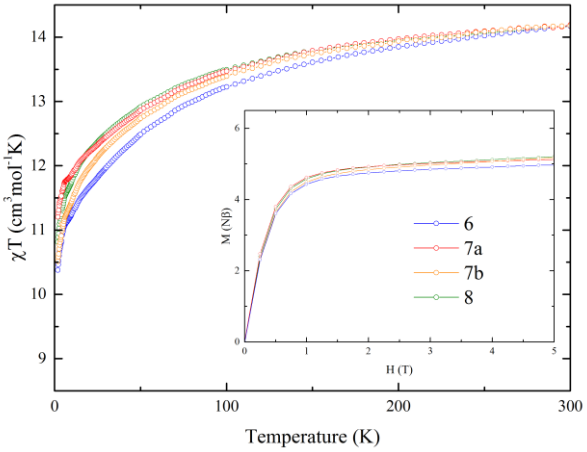

Figure 10. T dependence of χT and the field dependence of the magnetization at 1.85 K (insert).

Dynamic magnetic properties in the solid state. All complexes exhibit similar behavior with an out-of-phase signal (χ") in the high frequency region without an external *dc* magnetic field (Figure 11). We were able to fit the experimental data (Table S3 for **6**, Table S5 for **7a**, Table S7 for **7b** and Table S9 for **8**) and extract relaxation times (τ) (Figure 12) by transposing the Cole-Cole equation (equation 1):[18]

$$\chi^{i} = \chi_{adia} + \frac{\chi_{iso} - \chi_{adia}}{1 + (i2\pi\nu\tau)^{1-\alpha}} \quad (1)$$

$$\tau^{-1}(T, H) = AT^{2}H^{4} + CT^{m} + \tau_0^{-1}\exp\frac{-\Delta}{k_B T} + QTM^{-1} \quad (2)$$

$$\chi^{i} = \chi_{adia} + \frac{\chi_{iso} - \chi_{adia}}{\left\{1 + (i2\pi\nu\tau)^{1-\alpha}\right\}^{\beta}} \quad (3)$$

The complex susceptibility χ^i depends on the isothermal (χ_{iso}) and adiabatic (χ_{adia}) susceptibilities, the frequency (ν), τ and the dispersion parameter of τ (α). From equation 2,[19] at low T, the magnetic relaxation of the four complexes is dominated by quantum tunneling of the magnetization (QTM) with τ values of 3.43×10^{-5} s, 2.85×10^{-4} s, 2.40×10^{-5} s, 6.17×10^{-6} s and 1.59×10^{-5} s for **6**, **7a**_1, **7a**_2, **7b** and **8**, respectively (Table 3). Magnetic relaxation of complex **7a** is slower than the other complexes. At higher T, an Orbach process became predominant with energy barriers of 38.4 cm^{-1}, 10.2 cm^{-1}, 13.1 cm^{-1}, 19.1 cm^{-1} and 23.6 cm^{-1} for **6**, **7a**_1, **7a**_2, **7b** and **8**, respectively.

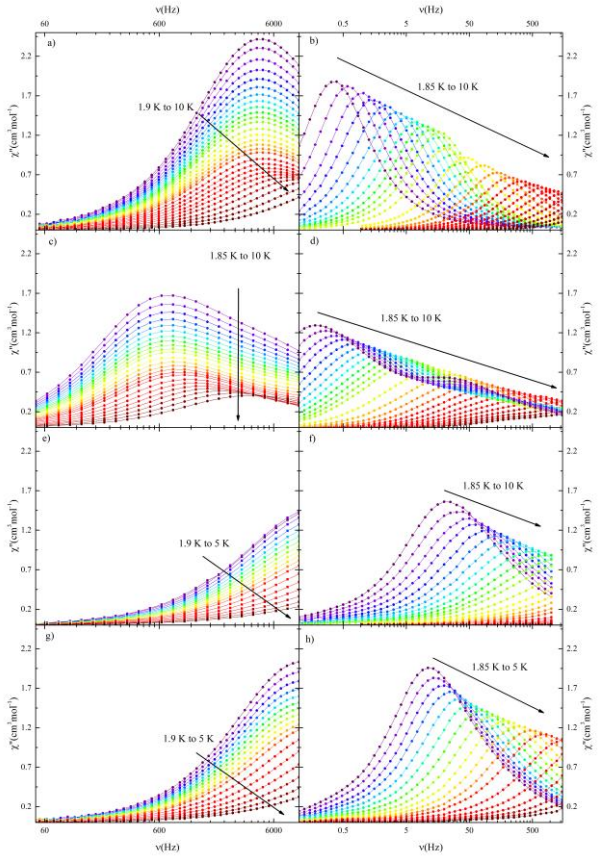

Figure 11. T and υ dependences of χ'' of (a, b) **6**, (c, d) **7a**, (e, f) **7b** and (g, h) **8** at (a, c, e, g) 0 Oe and (b, d, f, h) 1000 Oe.

In order to suppress QTM, the optimum external *dc* field for each complex was determined to be 1000 Oe (Figure S3). This field efficiently suppresses QTM for the three complexes. In addition, the magnetic relaxation for **6** and **8** was determined to be a single process governed by Raman and Orbach mechanisms for **6** and direct, Raman and Orbach mechanisms for **8**. For **7a**, two processes occur (Figure S4). The faster one is governed by direct and Orbach mechanisms, and the slower one is governed by Raman and Orbach mechanisms. The differences among the complexes remain unclear at this point, but we think that the differences originate from the following: i) The asymmetric unit of **7a** is composed of two independent molecules, and each of them relax by a different pathway, whereas the other complexes have only one molecule in their asymmetric units. ii) In **7a**, the bromo-thiophene ring is disordered over two positions, and each of them relax differently, whereas the other complexes did not show any disorder. iii) The Dy^{III} ions are the same, and they have two pathways for relaxation available at low T due to small energy splitting between two m_J levels. The energy barrier observed with or without a field is slightly different due to the fact that, in our complexes, the Orbach mechanism is observed only at high ν, and is combined with another mechanism. Thus, it is not certain that the Orbach process is dominant in the available ν range.

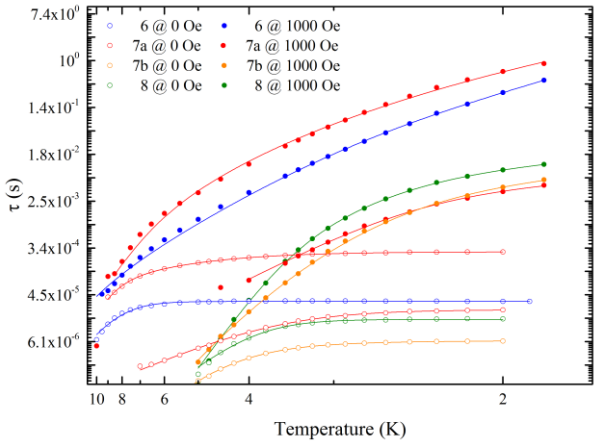

Figure 12. Arrhenius plots with best-fit curves (lines) for the complexes in the solid state at 0 Oe (open circles) and 1000 Oe (filled circles).

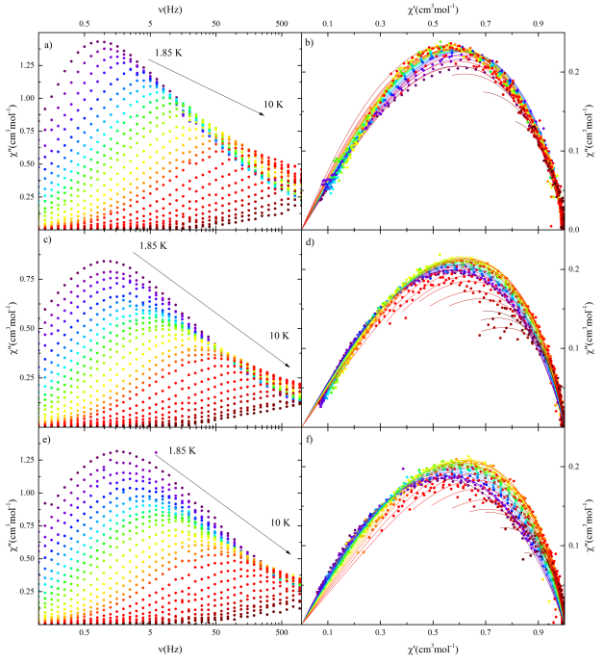

Figure 13. T and ν dependences of χ'' at 1000 Oe for (a) **6**, (c) **7**, and (e) **8** and the corresponding normalized Cole-Cole plot for (b) **6**, (d) **7**, and (f) **8** with the lines representing the results from the fittings.

In order to clarify the roles of the packing structure and the substitutents, saturated CH_2Cl_2 solutions of each complex were prepared, and their dynamic magnetic properties were investigated in a field of 1000 Oe, which was used for the solid-state measurements. A procedure previously reported by Pointillard *et al.* was used.[5] The stabilities of the complexes in solution were confirmed by the presence of new peaks in the absorption spectra after coordination of the ion. A saturated solution of the complexes was quenched to avoid precipitation.

The three complexes showed similar behavior to each other (Figures 13 and 14). However, the solution magnetic data could not be fit by using the Cole-Cole equation to extract τ due to the asymmetry of the peaks (Figure S6). The data were fit by combining two Cole-Cole equations. However, the parameters had significant error, which was potentially bigger than the values of the parameters

themselves. This problem was solved by using the Havriliak-Negami model (Equation 3).[20] Similar to the Cole-Cole model, the Havriliak-Negami model was initially used to analyze the dielectric properties of polymers. This model introduces an additional parameter β, which can take any value between 0 and 1, making it possible to fit asymmetric relaxation data (Figure S7). The physical meaning of this parameter (ν dependence of the magnetic permittivity, magnetic viscosity, ...) remains under consideration. The Cole-Cole model is recovered when $\beta = 1$. It should be noted that the τ values obtained by using this model are longer than those obtained from the peak maximum of χ''.

In solution, the relaxation processes of **6** and **7** are governed by direct and Orbach processes, whereas **8** is governed by Orbach and Raman processes and QTM (Table 3). In addition, τ_0 is significantly high in solution in a 1000 Oe field.

The magnetic properties of lanthanide ions are affected by the crystal field, which is generated mainly by the coordinated atoms, according to their relative positions and charges. Compared to the solution state, the crystalline state induces additional constraints on the coordination sphere due to the interactions among neighboring molecules. In the solution state, the coordination sphere around the Dy ion in **6**, **7** and **8** are similar and close to the gas phase. This similarity is evidenced by the complexes having nearly the same τ at any T. Thus, the substitution of one proton of the thiophene ring, which is not involved in the coordination of the Dy ion, with bromide or an acetylene group does not have an effect on the slow relaxation of the ion and cannot be used to directly tune the magnetic properties of SMMs. Nevertheless, distal substitution can indirectly be used to adjust the slow magnetic relaxation of SMMs by changing the crystal packing of the molecule and consequently changing the constraints on the coordination sphere. This is particularly visible for complex **7**. The polymorph **7a** crystallized in the space group $P2_1/n$ with two molecules in the asymmetric unit and two values of τ, whereas **7b** crystallized in the space group $P2_1/a$ with one molecule in the asymmetric unit and one τ value. Changing the packing mode of a complex can play a greater role in the tuning of magnetic properties than distal substitution can.

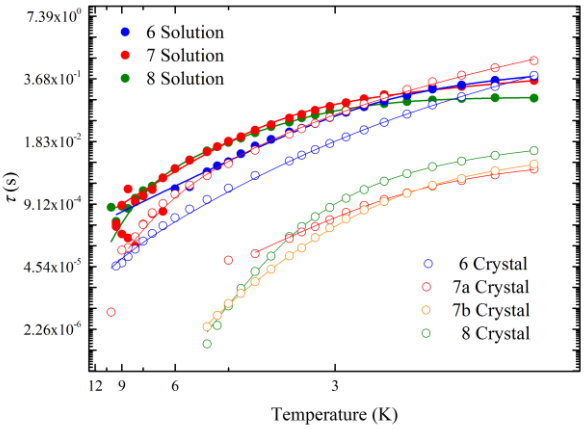

Figure 14. Arrhenius plot with best-fit curves (lines) for the three complexes in the solid (open circles) and solution (filled circles) states at 1000 Oe.

Table 3. Summary of the fitting parameters for equation 2 for τ *vs.* T.

	Direct Process	Orbach Process		Raman process		QTM
Parameter (unit)	A ($s^{-1}K^{-2}$)	τ_0 (s)	Δ (cm^{-1})	C ($s^{-1}K^{-m}$)	m	s
6 @ 0 Oe	—	$4.43 \times 10^{-8} \pm 1.39 \times 10^{-8}$	38.3 ± 2.6	—	—	$3.43 \times 10^{-5} \pm 1 \times 10^{-7}$
7a_1 @ 0 Oe	—	$2.56 \times 10^{-5} \pm 1.0 \times 10^{-6}$	10.2± 0.1	$3.95 \times 10^{-5} \pm 1.3 \times 10^{-6}$	9	$2.85 \times 10^{-4} \pm 6 \times 10^{-7}$
7a_2 @ 0 Oe	—	$1.34 \times 10^{-7} \pm 9 \times 10^{-9}$	13.1 ± 0.2	—	—	$2.40 \times 10^{-5} \pm 1 \times 10^{-7}$
7b @ 0 Oe	—	$5.66 \times 10^{-9} \pm 1.26 \times 10^{-9}$	19.1 ± 0.6	—	—	$6.17 \times 10^{-6} \pm 5 \times 10^{-8}$
8 @ 0 Oe	—	$2.70 \times 10^{-9} \pm 8.2 \times 10^{-10}$	23.6 ± 0.8	—	—	$1.59 \times 10^{-5} \pm 1 \times 10^{-7}$
6 @ 1000 Oe	—	$3.03 \times 10^{-5} \pm 4.1 \times 10^{-6}$	14.8 ± 0.3	$8.60 \times 10^{-2} \pm 2.6 \times 10^{-3}$	5	—
7a_1 @ 1000 Oe	—	—	—	$3.65 \times 10^{-2} \pm 5 \times 10^{-4}$	5.5	—
7a_2 @ 1000 Oe	$5.69 \times 10^{-11} \pm 1.2 \times 10^{-12}$	$3.47 \times 10^{-7} \pm 7.0 \times 10^{-8}$	15.6 ± 0.4	—	—	—
7b @ 1000 Oe	$3.88 \times 10^{-11} \pm 1.1 \times 10^{-12}$	$1.49 \times 10^{-9} \pm 9.0 \times 10^{-10}$	30.6 ± 1.9	$1.13 \times 10^{-1} \pm 6 \times 10^{-3}$	9	—
8 @ 1000 Oe	$2.13 \times 10^{-11} \pm 2 \times 10^{-13}$	$9.21 \times 10^{-12} \pm 6.53 \times 10^{-12}$	43.2 ± 1.8	$4.02 \times 10^{-2} \pm 7 \times 10^{-4}$	9	—
6 Sol @ 1000 Oe	$6.77 \times 10^{-13} \pm 5 \times 10^{-15}$	$5.26 \times 10^{-5} \pm 6.9 \times 10^{-6}$	15.7 ± 0.3	—	—	—
7 Sol @ 1000 Oe	$1.37 \times 10^{-13} \pm 5 \times 10^{-15}$	$2.33 \times 10^{-4} \pm 4.2 \times 10^{-5}$	20.4 ± 0.7	—	—	—
8 Sol @ 1000 Oe	—	$2.44 \times 10^{-3} \pm 3.5 \times 10^{-4}$	12.6 ±0.5	$9.95 \times 10^{-7} \pm 4.33 \times 10^{-7}$	9	$9.60 \times 10^{-1} \pm 7 \times 10^{-3}$

4. Conclusion

Three complexes (complex **6**, **7** and **8**) were prepared, and two polymorphs of **7** were isolated. The complexes crystallized in monoclinic space groups with columnar structures and one molecule per asymmetric unit, except for complex **7a,** which had two independent molecules per asymmetric unit. This difference is reflected in the dynamic magnetic measurements. Only one relaxation processes were observed for complexes **6**, **7b** and **8**, whereas two relaxation processes were observed for the complex **7a**. The differences in the magnetic properties were explained by the differences in the packing structures. The results of solution-state magnetic measurements confirmed that the packing structure had an effect on the magnetic properties because all three complexes exhibited similar magnetic behavior.

Because the Cole-Cole model could not be used to fit the solution-state data, the Havriliak-Negami model was used. The Havriliak-Negami model introduces an additional parameter β which makes it possible to fit an asymmetric relaxation peak with a "tail" in the high ν range. In order to confirm the role played by distal substitution on the magnetic properties of the Dy ion, we are currently preparing a series complexes with different substitutents, such as electronegative (chloride, iodide, methoxy, etc.) and electropositive groups (nitro, etc.), on the thiophene ring.

References

1. R. Sessoli, L. Hui, A. R. Schake, S. Wang, J. B. Vincent K. Folting, D. Gatteschi, G. Christou, *J. Am. Chem. Soc.* **1993**, 115, 1804.
2. R. Sessoli, D. Gatteschi, A. Caneschi, M. A. Novak, *Nature* **1993**, 365, 141.

3. N. Ishikawa, M. Sugita, T. Ishikawa, S. Koshihara, Y Kaizu, *J. Am. Chem. Soc.* **2003**, 125, 8694.
4. D. Zeng, M. Ren, S-S. Bao, L-M. Zheng, *Inorg. Chem.* **2014**, 53, 795.
5. G. Cosquer, F. Pointillart, S. Golhen, O. Cador, L. Ouahab, *Chem. Eur. J.* **2013**, 19, 7895.
6. V. Mereacre, A. Baniodeh, C. E. Anson, A. K. Powell, *J. Am. Chem. Soc.* **2011**, 133, 15335.
7. G. Cosquer, F. Pointillart, J. Jung, B. Le Guennic, S. Golhen, O. Cador, Y. Guyot, A. Brenier, O. Maury, L. Ouahab, *Eur. J. Inorg. Chem.* **2014**, 69.
8. M. F. Richardson, W. F. Wagner, D. E. Sands, *J. Inorg. Nucl. Chem.* **1968**, 30, 1275.
9. CrystalClear-SM 1.4.0 SP1, Rigaku Corporation. **17 April 2008**, Tokyo, Japan.
10. A. Altomare, M. C. Burla, M. Camalli, G. L. Cascarano, C. Giacovazzo, A. Guagliardi, A. G. G. Moliterni, G. Polidori, R. Spagna, *J. Appl. Crystallogr.* **1999**, 32, 115.
11. L. J. Farrugia, *J. Appl. Crystallogr.* **2012**, 45, 849.
12. G. M. Sheldrick, *Acta Cryst. C* **2015**, 71, 3.
13. G. A. Bain, J. F. Berry, *J. Chem. Educ.* ***2008***, 85, 532−536.
14. (a) A. Ruiz-Martínez, D. Casanova, S. Alvarez, *Chem. – Eur. J.*, **2008**, 14, 1291. (b) S. Alvarez, P. Alemany, D. Casanova, J. Cirera, M. Llunell, D. Avnir, *Coord. Chem. Rev.*, **2005**, 249, 1693.
15. G. Cosquer, F. Pointillart, B. Le Guennic, Y. Le Gal, S. Golhen, O. Cador, L. Ouahab, *Inorg. Chem.*, **2012**, 51, 8488.
16. F. Gutierrez, C. Tedeschi, L. Maron, J.P. Daudey, R. Poteau, J. Azema, P. Tisnes, C. Picard, *Dalton Trans.*, **2004**, 1334.
17. O. Kahn, Molecular Magnetism; *VCH Publishers*: Weinheim, Germany, **1993**.
18. K. S. Cole, R. H. Cole, *J. Chem. Phys.* **1941**, 9, 341.
19. K.S. Pedersen, L. Ungur, M. Sigrist, A. Sundt, M. Schau-Magnussen, V. Vieru, H. Mutka, S. Rols, H. Weihe, O. Waldmann, L.F. Chibotaru, J. Bendix, J. Dreiser, *Chem. Sci.*, **2014**, 5, 1650.
20. S. Havriliak, S. Negami, *Polymer*, **1967**, 8, 161.

Graphical Abstract

Packing Structure Effects on the Slow Magnetic Relaxation Pathways of Dysprosium (III) Complexes

Mritunjoy Kamila, Goulven Cosquer, Brian K. Breedlove, Masahiro Yamashita

Four complexes were synthesized to investigate the effects of distal substituents on the magnetic properties of the dysprosium ion. Three over four complexes underwent slow magnetic relaxation with a single relaxation time, and two relaxation times for the last one. To clarify the role of distal substitution and crystal packing, the magnetic properties were studied in solution.